

https://dspace.org/

The water-gas shift deactivation studies

Mellor, John Ramsdon

2011-02-21
http://hdl.handle.net/10539/9057

Downloaded from a DSpace repository. https://dspace.org/

3.2.4 Pulse chemisorption procedure

Figure 3.4 shows the valve positions necessary for pulse chemisorption.

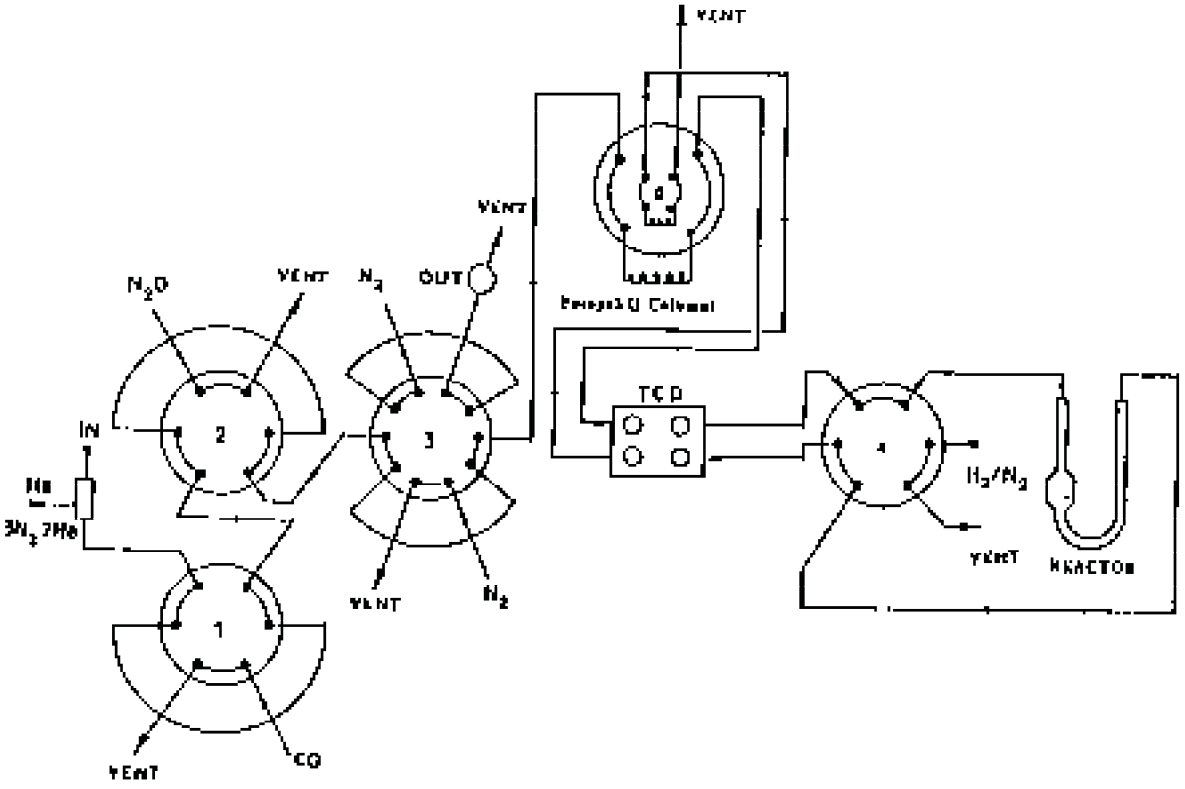


Figure 3.4 Schematic diagram of the pulse chemisorption apparatus, configured for nitrous oxide decomposition and carbon monoxide back titration (modified from reference 8)

Known volumes of nitrous oxide were consecutively injected into the helium carrier gas stream using valve No. 2 which was fitted with interchangeable calibrated sample loops. Valve No. 5 ensured that reactant and product gas passed through respective Porapack Q columns. The TCD detector polarity was reversed immediately after measurement of the reactant nitrous oxide, in order to utilise the same detector for product gas analysis. Reaction with the sample took place in a modified U-tube (previously described) positioned in the oven and controlled to within $\pm$ 1°C of the desired temperature. Excellent separation of unreacted nitrous oxide and nitrogen was obtained on the product Porapack Q column. The area of the nitrogen peak

was used to calculate the extent of nitrous oxide decomposition as it was found to be more accurate than measuring the differences between the areas of inlet and outlet nitrous oxide peaks. Calibration was achieved by measuring the areas of known volumes of nitrogen to within 10% of the measured sample area. A sample of nitrogen calibrating gas was withdrawn by a syringe (Supelco, USA) from the septum labelled "OUT" and injected into the septum labelled "IN". Provision for quick, efficient calibration of routine samples of a known surface area range was provided by injecting nitrogen from interchangeable calibrated sample loops fitted to valve No. 3. The volume of nitrogen liberated as a result of the N_2O decomposition (V_R) was obtained from Equation 3.5:

$$V_R = V_{cal} \frac{A_R}{A_{cal}} \qquad - (3.5)$$

where: V_{cal} = calibration gas volume (ml)
A_R = peak area of product gas produced by reaction
A_{cal} = calibration peak area

3.2.5 CO-Back titration procedure

The procedure for determining copper surface area by carbon monoxide back titration was similar to that employed for pulse chemisorption (see Figure 3.4). In this case known volume(s) of CO gas from interchangeable calibrated sample loops were injected into the helium carrier gas using valve No. 1. The Porapack Q column provided good separation of CO and CO_2.

Carbon monoxide back titrations were performed at 200°C, rather than 150°C or 240°C as proposed by Koeppel *et al.* (13) and Chinchen *et al.* (6) respectively. This temperature was chosen because DSC experiments showed that no phase transitions associated with CO reduction occurred

above 160°C for the ICI 53-1 commercial catalyst, Raney and co-precipitated catalysts described in Section 3.2.2.

The CO_2 peak area was used to quantify the oxygen removed from the copper surface during reduction, as it proved more accurate than measuring the difference between the areas of inlet and outlet CO peaks. Using a gas syringe, known volumes of CO_2 were injected into the "IN" septum. In order to minimize errors, only calibration areas within 10% of the measured sample area were accepted. Equation 3.4 was used to calculate the volume of CO_2 formed by reduction.

3.2.6 Single point BET determination

The sample BET surface area was determined by the repetitive adsorption/desorption cycling method described by Nelson and Eggertsen (15). A 30% nitrogen in helium mixture (25ml/min) was used as the carrier gas because Lowell (16) suggested that a relative nitrogen pressure of 0.3 gives BET surface areas in close agreement with the multipoint method. A continuous flow system was achieved by isolating the two Porapack Q columns by switching valve No. 4 to the position demonstrated in Figure 3.2. Calibration by nitrogen was carried out using the procedure described in Section 3.2.4. A 100Ω platinum wire resistor was repeatedly used to show that the liquid nitrogen temperature did not fluctuate by more than ± 0.2K during measurement. This change did not alter the nitrogen vapour pressure significantly enough to cause inaccurate BET results. Before reduction or surface area determination, samples were dried in a vacuum oven at 110°C for 2 hours, and outgassed at 150 - 200°C under He or N_2 for at least 2 hours, to provide a clean surface area. Several values obtained from the single point flow method were compared with measurements made using a Quantasorb Sorption System (ENERTEK, CSIR, South Africa) and found to agree within ± 3%.

3.3 RESULTS AND DISCUSSION

3.3.1 Calculation of copper surface area

If complete coverage of the copper surface via Reaction 3.2 is assumed, then the volume of nitrous oxide decomposed for the average site densities of 1.68, 1.46 and 1.35 x 10^{19} Cu atoms.m^{-2} (see Section 3.1) are 0.313, 0.271 and 0.251 ml$_{N_2O}$ m^{-2} at STP. The copper surface areas were calculated by dividing the experimentally determined volume of decomposed nitrous oxide by these values. The calculation may be summarized by the following equations:

The volume of nitrous oxide (ml) reacted was converted to STP according to Equation 3.6.

$$V_{N_2O}(STP) = \frac{P_A \cdot 273\,K}{T_R \cdot 760\,mmHg} \cdot \frac{A_R}{A_{cal}} \cdot V_{cal} \qquad - (3.6)$$

where: P_A = ambient pressure (mmHg)
T_R = temperature of chemisorption (K)
A_R = peak area of nitrogen produced by reaction
A_{cal} = calibration peak area
V_{cal} = calibration gas volume (ml)

Copper surface area ($m^2.g^{-1}$) may be calculated from Equation 3.7:

$$S_{Cu} = \frac{V_{N_2O}(STP)}{m.V'_{N_2O}(STP)} \qquad - (3.7)$$

where: m = mass of sample (g)
$V'_{N_2O}(STP)$ = Theoretical STP volume of nitrous oxide consumed per m^2 as calculated from approximations for the surface areas of the (100), (110) and (111) planes. $V'_{N_2O}(STP)$ = 0.313, 0.271 or 0.251 ml.m^{-2}.

In some cases results were expressed as a surface coverage, θ (see Section 3.1) as determined according to Equation 3.4.

3.3.2 Mass dependence and order of analysis

The dependence of the technique on sample mass was initially investigated using the copper powder sample. Table 3.1 shows the copper powder surface coverage, θ, as determined for the three conflicting values of average site density, for increasing sample masses. The experiment was conducted at 90°C which Evans et al. (8) cited as the optimum temperature for complete monolayer coverage using a pulse chemisorption technique. The single point BET surface area of reduced copper (prior to chemisorption) and oxidised copper (after chemisorption) was determined for the same sample of mass greater than 0.9g and found to be 2.37 and 2.26 $m^2.g^{-1}$ respectively. A standard deviation of $\pm$ 3% applied to both measurements. Replicate experiments showed that the standard deviation of the relative copper surface areas were $\pm$ 4% for the entire sample mass range considered. Unreduced copper oxide produced no N_2O decomposition under the same conditions.

Table 3.1 **Metal surface coverage (θ) as a function of sample mass and order of analysis**

Mass (g)	Order of Analysis		θ		
	(i)	(ii)	a	b	c
0.2473	Chemisorption	BET	0.35	0.41	0.44
0.3290	Chemisorption	BET	0.53	0.61	0.66
0.6204	Chemisorption	BET	0.54	0.63	0.68
0.9301	Chemisorption	BET	0.79	0.91	0.98
1.0286	Chemisorption	BET	0.77	0.89	0.97
0.9782	BET	Chemisorption	0.38	0.44	0.47

a: Assuming 1.68×10^{19} copper atoms.m^{-2}
b: Assuming 1.46×10^{19} copper atoms.m^{-2}
c: Assuming 1.35×10^{19} copper atoms.m^{-2}

A value of 0.251ml (STP) N_2O m^{-2} gives the closest agreement to unit coverage, $\theta = 1$, (expected at 90°C by Evans *et al.* (8)) for a sample mass greater than 0.9g. Based on this value, the copper surface area as a function of sample mass has been plotted in figure 3.5.

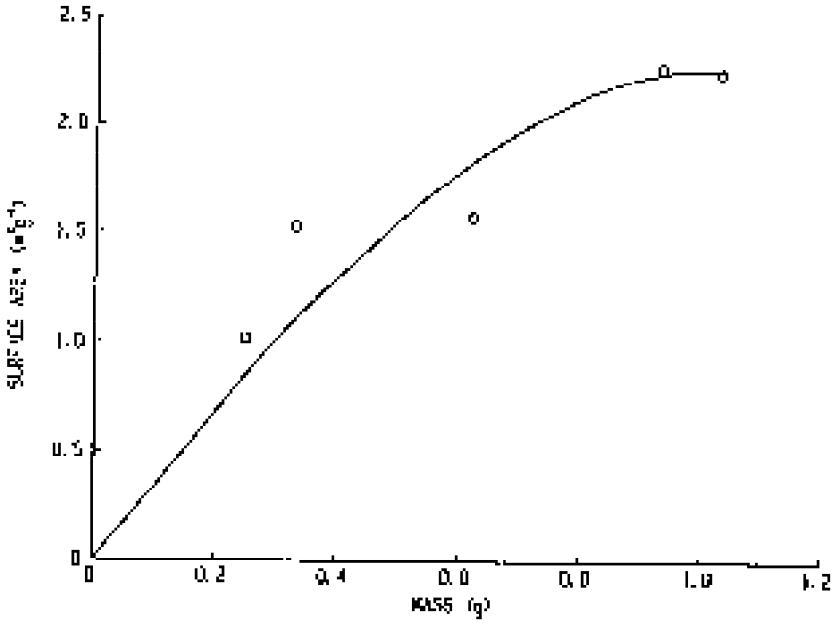


Figure 3.5 Surface area ($m^2.g^{-1}$) of copper powder as a function of mass

The copper powder surface area significantly decreased when sample masses fell below ± 0.90g, clearly indicating that measurement inaccuracies are greater when smaller masses of low surface area samples are used. A similar surface area decrease below a critical sample mass of 50mg was observed by Meyers *et al.* (17) during the determination of the Pt surface area of a 0.74% Pt/Al_2O_3 catalyst by CO chemisorption. They concluded that trace impurities in their He carrier gas accounted for the effect.

From Table 3.1 it can be seen that reversing the order of analysis, (i.e. determining the BET surface area of a reduced sample *before* N_2O pulse chemisorption) resulted in a substantial decrease in N_2O decomposition, even above the critical sample mass of ± 0.90g. The possibility of a

trace oxygen impurity in the carrier gas mixture (in spite of the purification methods employed) might have resulted in partial surface oxidation which would have considerably reduced the extent of N_2O reaction, but would not necessarily have altered the BET area significantly, as has been proved. Thus, for all results reported, pulse chemisorption experiments were conducted *before* BET surface area determination, or else the sample was reduced prior to both analyses. Also, catalyst masses were selected in the range 0.3 to 2g depending on their estimated copper areas.

3.3.3 Temperature dependence

The dependence of the technique on N_2O reaction temperature was examined using large masses of copper powder. Nitrous oxide pulse chemisorption analysis on the sample reduced *in situ* (see Section 3.2.3) was followed by single point BET surface area determination. For a temperature range of 30 - 140°C the surface coverage, θ, was calculated using all three values of average site density reported in the literature (see Section 3.1) and the results are presented in Table 3.2.

Table 3.2 The effect of temperature on the metal surface areas of powdered copper

Temp. (°C)	V_{N_2O} (ml(STP)g^{-1})	S_{Cu}($m^2.g^{-1}$)			θ		
		a	b	c	a	b	c
30	0.360	1.151	1.331	1.436	0.51	0.58	0.63
60	0.456	1.456	1.681	1.816	0.57	0.66	0.72
90	0.585	1.87	2.159	2.332	0.77	0.91	0.98
120	0.817	2.610	3.015	3.255	1.13	1.3	1.40
140	1.504	4.807	5.55	5.994	1.87	2.16	2.33

a: Assuming 1.68×10^{19} copper atoms.m^{-2}
b: Assuming 1.46×10^{19} copper atoms.m^{-2}
c: Assuming 1.35×10^{19} copper atoms.m^{-2}

From Table 3.2 it can be seen that a surface coverage of less than 100% is obtained for the temperatures evaluated up to 60°C. Temperatures between 90 and 120°C give the closest agreement to unit coverage for all values of average site density reported. However, the best agreement of $\theta = 0.98$ was found at a temperature of 90°C for a surface density of 1.35×10^{19} atoms.m^{-2} calculated on the basis of the three planes of copper being equally present, and assuming a mean area per copper site of 7.41 $Å^2$. Both the atomic density used by Evans *et al. (8)* and the value of 1.46×10^{19} atoms.m^{-2} proposed by Scholten and Konvalinka (1) led to copper surface areas much less than the BET surface area. Therefore, a surface density of 1.35×10^{19} atoms.m^{-2} was used to calculate the copper areas of catalysts from the volume of N_2O decomposed.

Figure 3.6 shows the effect of temperature on the decomposition of 1.94 ml N_2O pulses injected at 5 minute intervals over the copper powder sample.

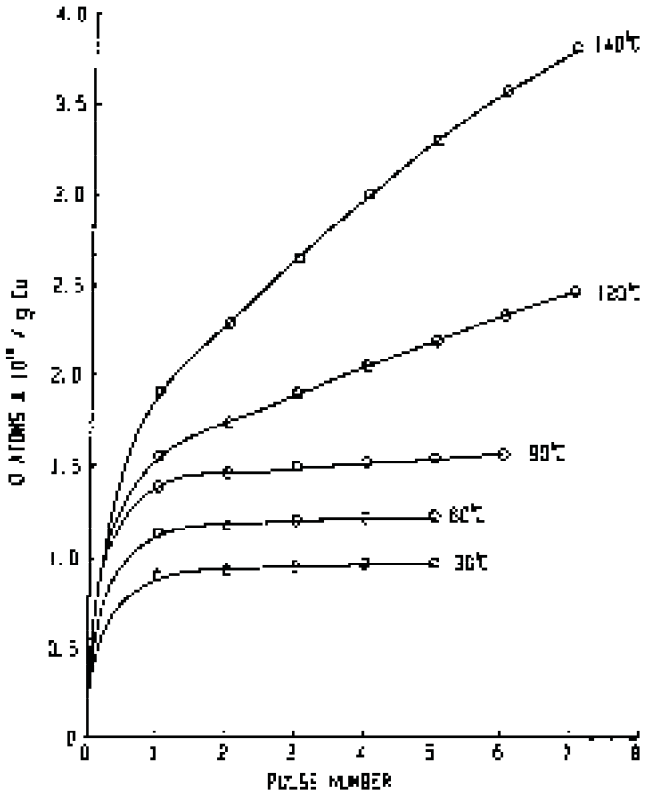


Figure 3.6 Adsorptive decomposition of nitrous oxide on a copper powder as a function of pulse number at various temperatures

Increasing the reaction temperature increases the surface coverage until unity is achieved around 90°C. This result is in accordance with Scholten *et al.* (3) who reported that the activation energy increased with coverage. Third and subsequent pulses at temperatures of 30, 60 and 90°C resulted in an *average* steady-state nitrous oxide decomposition of less than 2.5% of that consumed by the surface in the first pulse. This result may be explained by partial surface oxidation at temperatures less than 90°C and minimal bulk oxidation at a temperature of 90°C.

Our standard procedure of surface area determination at 90°C thus involved adding surface area contributions from N_2O pulses prior to the on-set of steady-state N_2O decomposition (see Table 3.3). Since steady-state N_2O decomposition is considered to be due to bulk oxidation, it is consequently of no significance to the surface calculation.

The *fraction* of the **combined** consumption of N_2O for the 2nd, 3rd, 4th and 5th pulses to that consumed by the surface in the first pulse increased from 41% at 120°C to 74% at 140°C. Considering that at both temperatures more than 50% of the nitrous oxide in the first pulse was unused, it is probable that not only does bulk oxidation take place at these elevated temperatures, but that the oxidation increases exponentially with increasing temperature. Scholten *et al.* (3) also observed an "oxygen break-through" (oxidation of the sub-surface layers) at temperatures of 120 and 140°C whilst Evans *et al.* (8) reported that bulk oxidation was clearly evident at 160°C, although their data suggested that bulk oxidation may have started to occur between 90 and 130°C.

3.3.4 The effect of catalyst support and pulse volume on bulk oxidation

The lack of N_2O decomposition over zinc oxide and alumina powders (Merk, AR grade) at 90°C confirmed that the

presence of these metal oxides in Raney and co-precipitated catalysts (see Section 3.2.3) did not contribute towards the specific surface area. Evans *et al.* (8) presented evidence to suggest that *bulk oxidation* was greatly enhanced in copper catalysts supported by zinc, aluminium and chromium oxides, whereas a silica supported catalyst and pure copper samples showed no decomposition of nitrous oxide in the second and subsequent pulses and hence no bulk oxidation characteristics. However, results presented in Figure 3.6 showed that repeated nitrous oxide pulse decomposition took place over the pure copper sample even at temperatures as low as 30°C.

Whilst it is not disputed that the presence of the abovementioned metal oxides may have encouraged bulk oxidation, it is suggested that the volume of nitrous oxide pulsed over supported and unsupported copper catalysts also promotes bulk oxidation at 90°C. Table 3.3 shows the copper surface areas of a Raney copper-zinc-aluminium catalyst obtained using multiple pulses of varying nitrous oxide volumes at 90°C.

Table 3.3 Metal surface areas ($m^2.g^{-1}$) of a Raney copper-zinc-aluminium catalyst using multiple pulses of varying N_2O volumes [a, b]

Pulse vol.(ml)	1.94		1.13		0.51	
Pulse No.	S_{Cu}	ΣS_{Cu}	S_{Cu}	ΣS_{Cu}	S_{Cu}	ΣS_{Cu}
1	18.0	18.0	13.7	13.7	7.0	7.0
2	0.8	18.8	3.6	17.3	6.7	13.7
3	0.2	19.0	0.6	17.9	3.3	17.0
4	0.1		0.3	18.2	0.7	17.7
5	0.07		0.2	18.4	0.5	18.2
6	0.09		0.1		0.3	18.5
7	0.1		0.06		0.1	
8	0.1		0.09		0.1	
9	- [c]		0.05		0.1	
10	-		0.03		0.1	

[a] Catalyst atomic composition = Cu(61.7) Zn(11.0) Al(25.9), S_{BET} = 34.3 $m^2.g^{-1}$, mass = 0.50g
[b] Period between pulses = 10 minutes
[c] Dashes indicate not measured

As expected, a decrease in pulse volume was accompanied by a corresponding increase in the number of pulses necessary to obtain unit coverage at 90°C. However, decreasing the N_2O pressure in the helium carrier gas stream also had the effect of promoting a steady-state partial oxidation of the bulk. From Table 3.3 it can be seen that similar copper surface area results were obtainable using comparatively large and small pulses of N_2O (surface areas differ by less than 2% of the mean 18.6 $m^2.g^{-1}$) as long as care was taken not to include area contributions from bulk oxidation. Evans *et al.* (8) reported that for nitrous oxide pulse volumes three to four times in excess of the amount consumed in the first pulse, Raney copper-zinc and chromium supported copper catalysts produced significant increases in N_2O decomposition with increasing time periods between pulses at a constant temperature of 90°C. This evidence supported their argument that the presence of other metal oxides (mentioned earlier) enhanced bulk oxidation. From Table 3.3 it can be seen that bulk oxidation from four consecutive 0.51ml N_2O pulses resulted in an additional "apparent" surface area of 0.4 $m^2.g^{-1}$ (corresponding to a 2.2% increase). The introduction of an additional single pulse after a period of 20 hours contributed only a further 0.1 $m^2.g^{-1}$ increase in the specific surface area of the Raney catalyst, which suggests that large partial pressures of N_2O in He rather than metal oxides may have caused bulk oxidation with time. Similar trends were observed for Raney Cu-Al and co-precipitated Cu-Zn-Al catalysts.

3.3.5 Carbon monoxide back titration

Carbon monoxide back titration was used to check the amount of oxygen chemisorbed on the copper surface from the decomposition of N_2O. (The method and procedure is described in Section 3.2.5). The reactions presented below were suggested by Habracken and Bootsma (16) to be facile:

$$CO(g) + Cu(s) \rightarrow CO(a) \qquad - (3.8)$$

$$CO(a) + O(s) \rightarrow CO_2(g) \qquad - (3.9)$$

where: a = adsorbed species

Table 3.4 lists the specific copper surface areas of three Raney copper catalysts prepared from alloys of varying compositions, a co-precipitated Cu-Zn-Aℓ catalyst and the ICI 53-1 commercial catalyst (see Section 3.2.2). These values were determined by pulse chemisorption at 90°C using a copper surface density of 1.35×10^{19} atoms.m^{-2} corresponding to 0.251ml (STP) $N_2O.m^{-2}$ (see Section 3.3.4). Also presented are the surface areas of the same catalysts calculated by pulsing 0.5ml volumes of CO at 200°C, until no further oxygen from the N_2O decomposition was observed to be liberated from the surface. A value of 0.251ml (STP)$CO_2.m^{-2}$ was used to calculate the CO back titrated copper surface areas.

Table 3.4 A comparison of the metal surface areas ($m^2.g^{-1}$) of copper-based catalysts determined by pulse N_2O decomposition and CO back titration

Sample	Chemisorption surface area	CO back titration surface area
Raney Cu-Aℓ [a]	8.3	7.7
Raney Cu-Zn-Aℓ [b]	16.9	17.6
Raney Cu-Zn-Aℓ [c]	18.9	18.2
Co-precipitated [d] Cu-Zn-Aℓ	5.3	4.9
ICI 53-1 [e]	10.2	9.3

[a] Atomic composition = Cu(70.2) Aℓ (29.8) $S_{BET} = 23.0 m^2.g^{-1}$
[b] Atomic composition = Cu(60.2) Zn (4.2) Aℓ (31.3) $S_{BET} = 33.4 m^2.g^{-1}$
[c] Atomic composition = Cu(61.7) Zn(11.0) Aℓ(25.9) $S_{BET} = 34.3 m^2.g^{-1}$
[d] Atomic ratio (Cu:Zn:Aℓ = 1:2.5:3), $S_{BET} = 85.9 m^2.g^{-1}$
[e] Atomic ratio (Cu:Zn:Aℓ = 1:1.2:1.6), $S_{BET} = 81.6 m^2.g^{-1}$

The results of both methods are within less than 9% of each other, which confirmed that pulse N_2O decomposition at 90°C is a valid and reliable technique for the determination of the copper surface areas of a variety of supported copper catalysts.

3.4 SUMMARY

It has been shown that an accurate estimate of the copper surface area of copper-based catalysts can be obtained using a single or number of nitrous oxide pulses at 90°C. An atomic density of 1.35×10^{19} atoms.m^{-2} gave the best results. The technique should be performed using a large sample mass to minimize errors of measurement, whilst carbon monoxide back titration is as an effective method for confirming copper surface area measurements.

3.5 REFERENCES

1. J.J.F Scholten and J.A. Konvalinka, *Trans. Faraday Soc.*, 65, (1969), 2465.

2. G.C. Bond and S.N. Namijo, *J. Catal.*, 118, (1989), 507.

3. J.J.F Sholten, A.P. Pijpers and A.M.L. Hustings, *Catal. Rev. - Sci. Eng.*, 27, (1985), 151.

4. J. Pritchard, T. Catterick, and R.K. Gupta, *Surf. Sci.*, 53, (1975), 1.

5. G.E. Parris and K. Klier, *J. Catal.*, 97, (1986), 374.

6. G.C. Chinchen, C.M. Hay, H.D. Vandervell, and K.C. Waugh, *J. Catal.*, 103, (1987), 79.

7. R.M. Dell, F.S. Stone, and P.F. Tiley, *Trans. Faraday Soc.*, 49, (1953), 195.

8. J.W. Evans, M.S. Wainwright, A.J. Bridgewater and D.J. Young, *Appl. Catal.*, 7, (1983), 75.

9. G. Sengupta, D.K. Gupta, M.L. Kundu and S.P. Sen, *J. Catal.*, 67, (1983), 223.

10. Th.J. Osinga, B.G. Linsen and W.P van Beek, *J. Catal.*, 7, (1967), 277.

11. E. Giamello, B. Fubini, P. Lauro and A. Bossi, *J. Catal.*, 87, (1984), 443.

12. B. Dvořák and J. Pašek, *J. Catal.*, 18, (1970), 108.

13. R.A. Koeppel, A. Baiker, Ch. Schild and A. Wokaun, in "*Preparation of Catalysts V*", (G. Poncelet, P.A. Jacobs, P. Grange and B. Delmon, eds.), Elsevier Science Publishers, Amsterdam, (1991), 53.

14. B.E. Sundquist, *Acta. Met.*, 12, (1964), 67.

15. F.M. Nelson and F.T. Eggertsen, *Anal. Chem.*, 30, (1958), 1387.

16. S. Lowell, "*Introduction to Powder Surface Area*", Wiley- Interscience, New York, (1979).

17. B.L. Meyers, R.S. Kurek and R.L. Mieville, J. Catal., 127, (1991), 788.

18. F.H.P.M. Habraken and G.A. Bootsma, *Surf. Sci.*, 88, (1979), 285.

CHAPTER FOUR

THE CHARACTERISATION, ACTIVITY AND STABILITY OF RANEY COPPER CATALYSTS FOR THE WATER-GAS SHIFT REACTION

4.1 INTRODUCTION

The ability to prepare a Raney copper catalyst with a composition similar to that reported for the conventional co-precipitated low temperature shift catalysts (see Chapter 1, Section 1.7) suggests that a Raney copper system may be active for the WGSR. This chapter considers the preparation and characterisation of these alloy-catalysts in order to obtain an understanding of their activity and stability.

4.1.1 Preparation and characterisation

The leaching process may be understood as the dissolution of a component or components from an alloy to produce a spongy porous material which may have catalytic potential primarily as a result of an increase in surface area of the active metal. Since, to a large extent, the leaching process determines the physical and chemical properties of the resultant catalyst, an investigation of this process is important to understand the unique way in which the Raney catalysts are formed. For this purpose, characterisation of the textural and structural properties of the resultant catalysts was carried out using AA, SEM, EDAX, XRD, pulse N_2O chemisorption, total BET surface area, pore volume and mean pore radii. In particular, characterisation studies are presented for the catalysts produced from a ternary alloy of nominal composition Cu(35) Zn(15) Aℓ(50). This alloy was chosen since Marsden et al. (1) reported that these Raney catalysts gave optimum methanol synthesis activity.

4.1.2 Activity and stability

From the work of Friedrich *et al.* (2) it may be deduced that Raney copper catalysts present certain hypothetical advantages over the co-precipitated catalytic alternatives. The authors reported that a fully extracted Raney catalyst of initial composition 96.9wt% Cu, 2.1wt% Zn and 1.5wt% Al showed little loss in methanol synthesis activity before steady-state conversion was attained. It was concluded that the residual zinc in Raney catalysts have some form of "stabilizing effect" on the catalysts. As the Raney copper catalyst was composed mainly of copper (96.9wt%), it was considered that the high BET surface area reported ($24.5\,m^2.g^{-1}$) corresponded almost entirely to copper crystallite surface area. Considering that high WGS activity for co-precipitated catalysts is achieved from a high specific copper surface area (see Chapter 1, Figure 1.6), it is reasonable to assume that the same correlation occurs for Raney copper catalysts. The substantial amount of support material necessary to stabilize the copper crystallites of co-precipitated catalysts (for example, 30 - 35% ZnO and 30 - 35% Al_2O_3 for the ICI 53-1 catalyst (3)) does not seem to be necessary in the Raney copper formulation. Rather, leached copper of high surface area appears, at least from the literature, to be stabilized by the continuous structure of Raney copper crystallites (4) and residual amounts of zinc (2) present in the porous leached zone.

The activity and stability of Raney copper catalysts for the WGSR was thus initially determined using the caustic leached Cu(35) Zn(15) Al(50) and Cu(50) Al(50) alloys, both of which will leave low or no Zn content after leaching.

The stabilizing influence of zinc in Raney copper catalysts was investigated by incorporating Zn^+ ions of varying dosages into the near-surface regions of caustic leached Cu(50) Al(50) alloys using ion implantation. This technique has the advantage of implanting concentrated pure

species with an accuracy and control that offers unprecedented freedom to modify both chemical and physical sub-surface and subsequent surface properties of a material (5).

Curry-Hyde *et al.* (6, 7) successfully demonstrated that it was possible to inhibit the zinc oxide dissolution mechanism by leaching alloys in presaturated zincate solutions. Initial experiments (6) using pellets of $CuAl_2$ showed that ZnO could be uniformly introduced to zinc free alloy catalysts by leaching in a zincate rich solution. Similarly, the leaching of ternary Cu-Zn-Al alloys in zincate/hydroxide solutions improved the catalyst zinc loading.

The "leaching/ZnO precipitation technique" (8) offers an economical, simple method to improve the zinc content of Raney copper catalysts. The effect of precipitated zinc enrichment on Raney copper activity and stability was evaluated with inference to catalyst morphology.

4.2 EXPERIMENTAL

Alloys, Raney copper catalysts and co-precipitated catalysts were prepared according to the detailed methods outlined in Chapter 2. Characterisation and activity studies were conducted on Raney catalysts prepared from 0.5 - 1.18mm alloy particles with nominal compositions of Cu(35) Zn(15) Al(50) - **Alloy C** and Cu (50) Al(50) - **Alloy D**. The alloy particles were leached in a 7.1M aqueous sodium hydroxide solution at 50°C (Chapter 2, Section 2.1.1). Extraction times used in the preparation of the catalysts from Alloy C were 1.0; 1.5; 2.0; 3.0 and 19.5 hours. Alloy D was extracted for 1.5 hours. Raney copper catalysts for ion implantation were prepared by the caustic leaching (7.1M) of alloy D particles (diameter 1.0 to 1.18mm) for one hour at 50°C.

Zinc enriched Raney copper catalysts were prepared

according to the procedure and conditions outlined for caustic leaching in Chapter 2, Section 2.1.1. In this case, three zincate/hydroxide solutions were used to leach Alloy C particles of diameter 0.5 to 1.180mm for a total extraction time of 2.0 hours at 50°C. The leach solutions were prepared by digesting the required amount of zinc nitrate (A.R. grade, Merk chemicals) in aqueous sodium hydroxide before addition to the alloy-water mixtures. The final leach solutions consisted of a hydroxide ion concentration of 7.1M and zincate concentrations of 0.1M, 0.5M and 0.75M.

The apparatus and techniques for the catalytic study have been discussed in detail in Chapter 2, Section 2.2. In all cases 2 ± 0.1ml of catalyst was loaded into the multi-fixed-bed laboratory reactors, reduced *in-situ*, and tested for WGS activity and time-on-stream stability under almost identical experimental conditions ($CO:H_2O$ = 1:22.5 temperature = 200°C and total GHSV = 1000h^{-1}). The catalysts were placed on-stream at the relevant start-up temperatures. Catalyst testing was conducted at atmospheric pressure (620mm/Hg in Johannesburg, South Africa). Also, blank thermal reactions in the absence of catalyst were found to be negligible, as was the formation of iron carbonyls in the stainless steel reactors.

4.3 RESULTS AND DISCUSSION

4.3.1 Characterisation

(a) The nature of Raney copper catalysts

The bulk analysis of the Alloys C and D of nominal composition Cu(35) Zn(15) Aℓ(50) and Cu(50) Aℓ(50), respectively, the base leached catalysts, the industrial ICI 53-1 catalyst and a co-precipitated WGS catalyst were determined by atomic absorption spectroscopy and the results are presented in Table 4.1. The atomic absorption analysis of the same catalysts after WGS activity and stability testing

Are also reported. As can be seen, within experimental limits, no change in catalyst composition occurs after WGSR.

Table 4.1 **Bulk compositions of fresh and used Raney copper catalysts of varying leach times**

Sample	Extraction time (h)	Composition before WGSR (wt%)			Composition after WGSR (wt%)		
		Cu	Zn	Al	Cu	Zn	Al
Alloy C	1.0	69.2	6.1	21.7	68.6	6.7	21.9
Alloy C	1.5	73.8	5.3	16.3	75.4	5.0	15.5
Alloy C	2.0	76.1	3.2	19.7	77.2	3.4	17.5
Alloy C	3.0	84.6	1.8	11.6	84.2	2.6	11.3
Alloy C	19.5	87.0	1.4	6.8	*		
Alloy D	1.5	84.7	0	15.3	86.3	0	13.0
ICI 53-1	-	25.8	31.8	17.9	26.2	32.5	19.4
Precip.	-	12.4	31.7	15.6	14.3	32.0	16.1

* Not measured

The Raney copper catalysts were analysed immediately after extraction and after reactor testing. For leaching times of one hour and longer the mass balance for the primary metals (copper, zinc and aluminium) was greater than 95%. The unaccounted mass is considered to be oxygen and in some cases a trace iron impurity. The approximate oxygen content of the unreduced fresh industrial ICI 53-1 catalyst (3) was calculated as 26.9%, which is in good agreement with the mass deficit of 24.8% determined from the AAS results reported in Table 4.2. The atomic ratio of Cu:Zn:Al before and after reactor testing was 1:1.2:1.6 and 1:1.2:2.2 respectively. Similarly, the atomic ratio of the co-precipitated catalyst for Cu:Zn:Al before and after

reactor testing was 1:2.5:3 and 1:2:3.6 respectively. As the catalyst rim could not be accurately removed from the alloy core for separate atomic absorption analysis, semi quantitative chemical compositions for the reacted rims and cores were calculated from more than two representative EDAX measurements, and the results are given in Table 4.2.

Table 4.2 **Rim and core compositions of Raney copper catalysts of varying leach times**

Sample	Extraction time (h)	Rim (wt%)			Core (wt%)		
		Cu	Zn	Al	Cu	Zn	Al
Alloy C	1.0	83.4	9.9	6.7	37.7	11.6	50.7
Alloy C	1.5	90.0	3.8	6.2	40.3	14.3	45.7
Alloy C	2.0	90.1	2.9	6.9	39.5	14.2	46.4
Alloy C	3.0	88.8	-	11.2	———		[b]
Alloy D	1.5	91.8	0	8.2	———		[b]

- Not detected
[b] No core observed from SEM

Good agreement between the EDAX and AA measurements for the determination of alloy core compositions were obtained.

SEM was used to obtain direct structural information on the morphological development and sintering phenomena of Raney copper catalysts produced from Alloy C. Elemental mapping provided a qualitative insight into the metal dispersion of the alloy and resultant catalysts. Figure 4.1 (i) shows the surface and cross-sectional area of Alloy C.

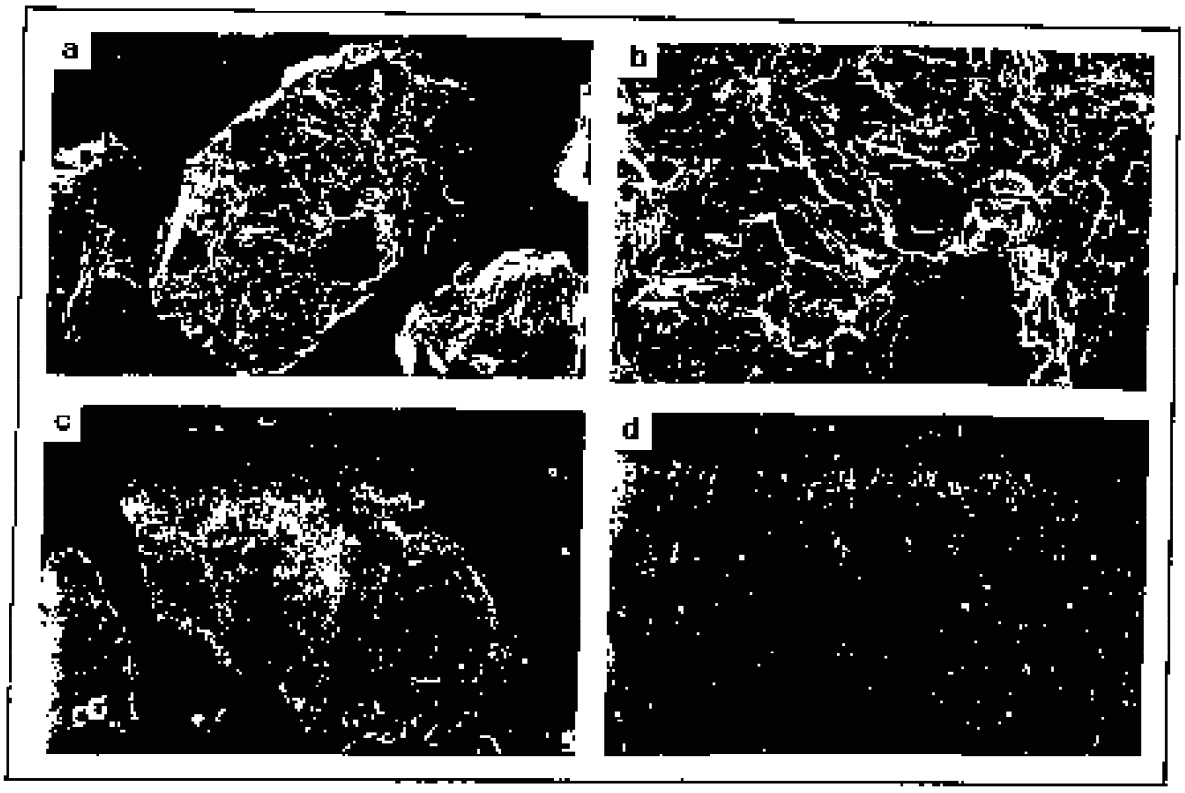


Figure 4.1 (i) Electron micrographs of the surface and cross-sectional area of Alloy C

a: Surface (MAG x 200)
b: Surface (MAG x 550)
c: Cross-section (MAG x 220)
d: Cross-section (MAG x 220)

Particles are roughly spherical (a and c) whilst the alloy surface (a and b) is non uniform, and not very porous ($S_{meas} < 3 m^2.g^{-1}$). In some cases cracks and fissures were apparent (a - d) and are considered to occur during rapid quenching of the melt or from the stress associated with alloy crushing to obtain required particle sizes (see Chapter 2). The cross-sectional electron micrographs (c and d) show the "compactness" of the cast alloy structure. From the elemental mapping micrographs, (Figure 4.1 (ii)) an even bulk dispersion of Cu, Zn and Al in Alloy C was observed.

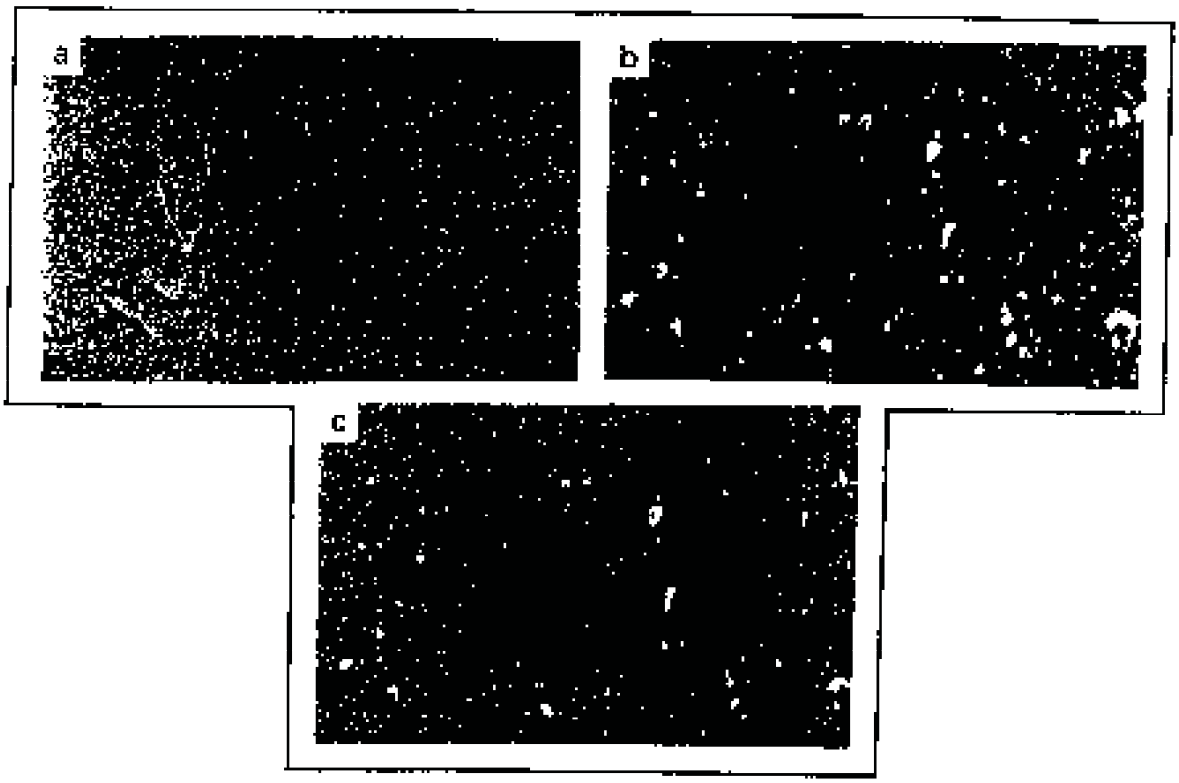


Figure 4.1 (ii) Cross-sectional copper, zinc and aluminium mapping of Alloy C

a: Cu mapping (MAG x 550)
b: Zn mapping (MAG x 550)
c: Al mapping (MAG x 550)

Figures 4.2 (i) - (ii) and 4.3 (i) - (ii) show electron micrographs of the surface of Raney copper catalysts before and after reactor testing respectively.

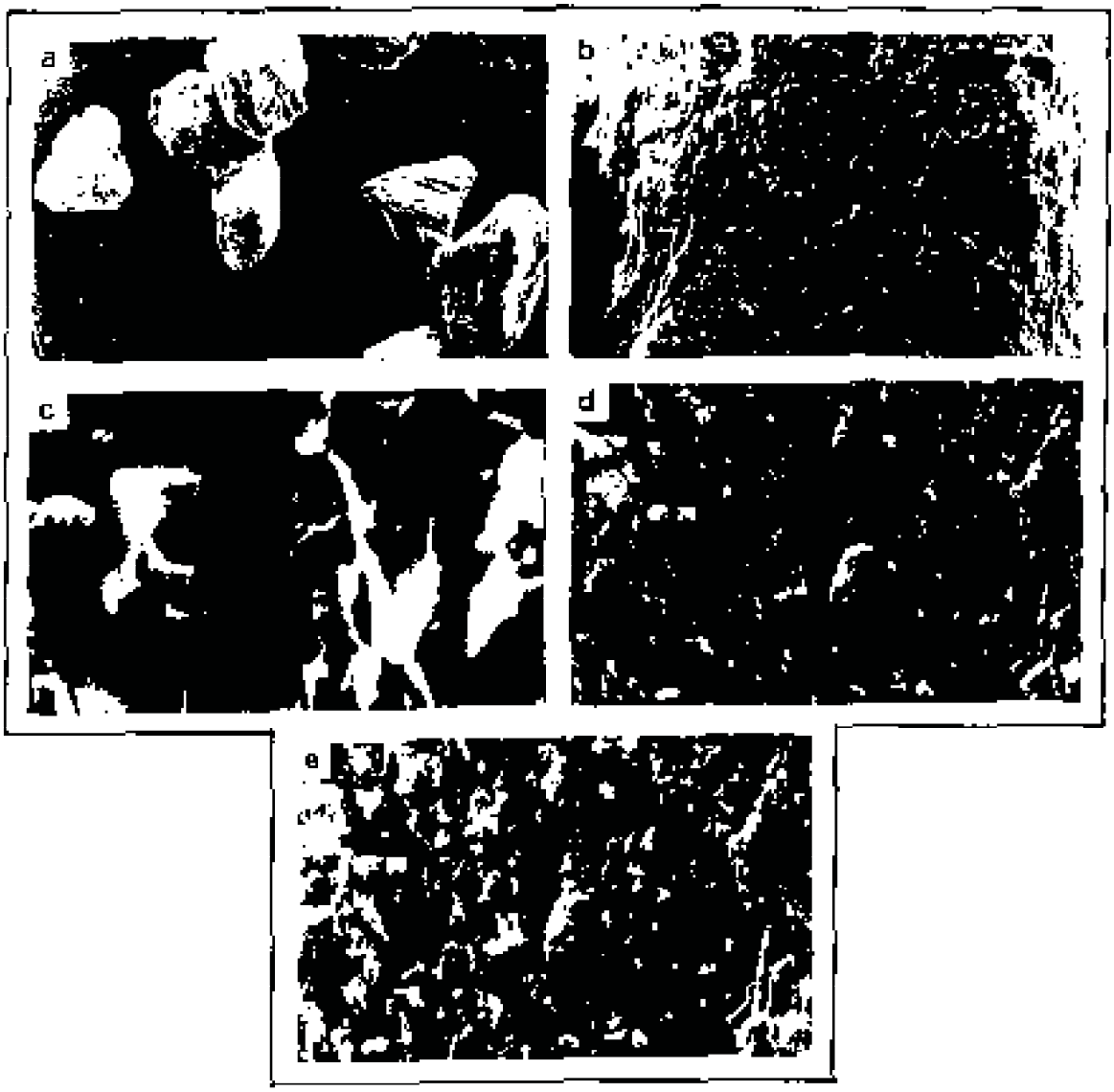


Figure 4.2 (i) Electron micrographs of the surface of a one hour leached Alloy C catalyst before WGSR

a: MAG x 30
b: MAG x 200
c: MAG x 2000
d: Zn mapping (MAG x 550)
e: Al mapping (MAG x 550)

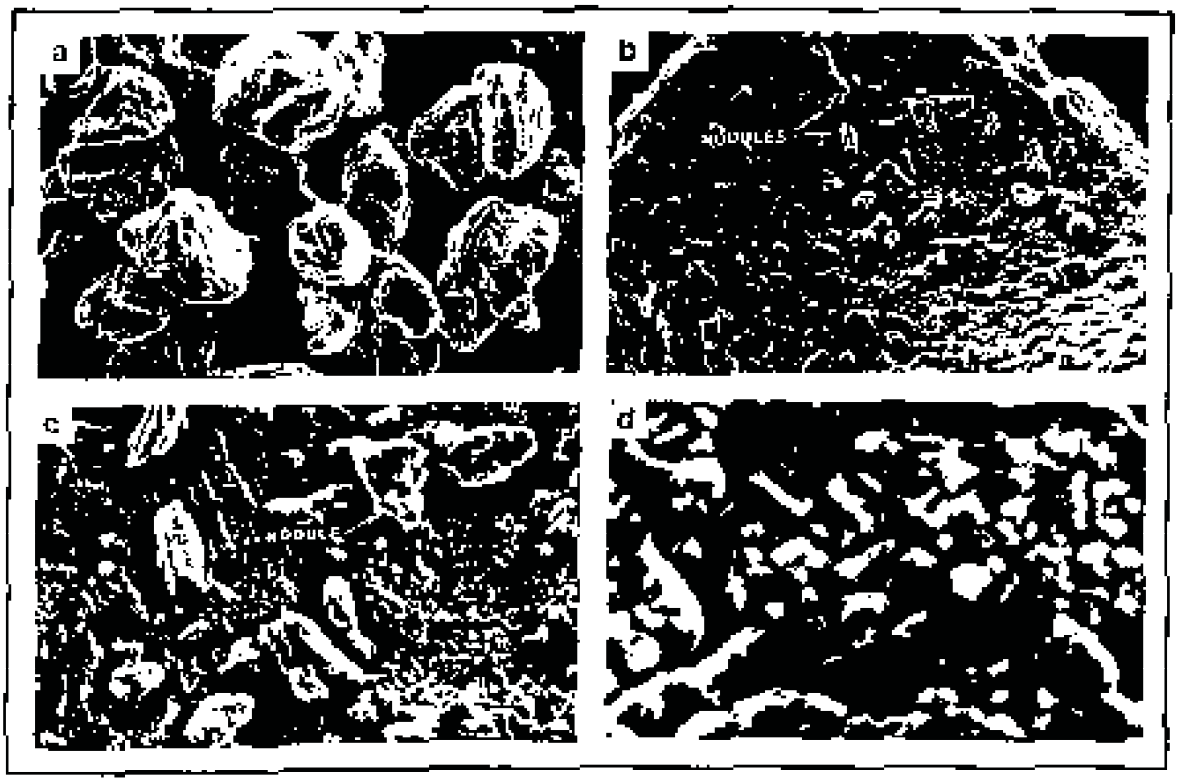


Figure 4.2 (ii) Electron micrographs of the surface of a three hour leached Alloy C catalyst before WGSR

a: MAG x 30
b: MAG x 200
c: MAG x 550
d: MAG x 2000

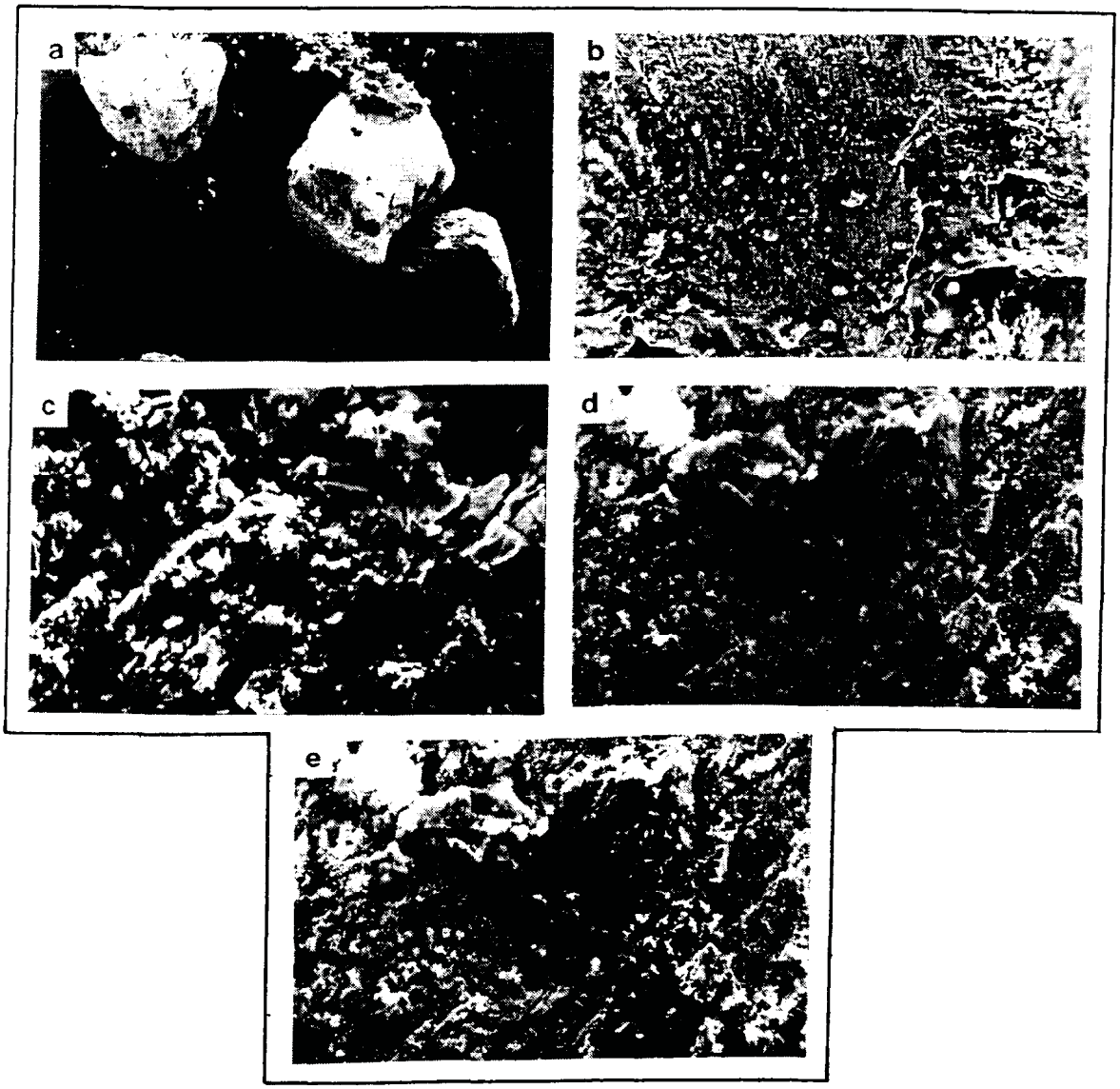


Figure 4.3 (i) Electron micrographs of the surface of a one hour leached Alloy C catalyst after WGSR

a: MAG x 30
b: MAG x 200
c: MAG x 2000
d: Zn mapping (MAG x 550)
e: Aℓ mapping (MAG x 550)

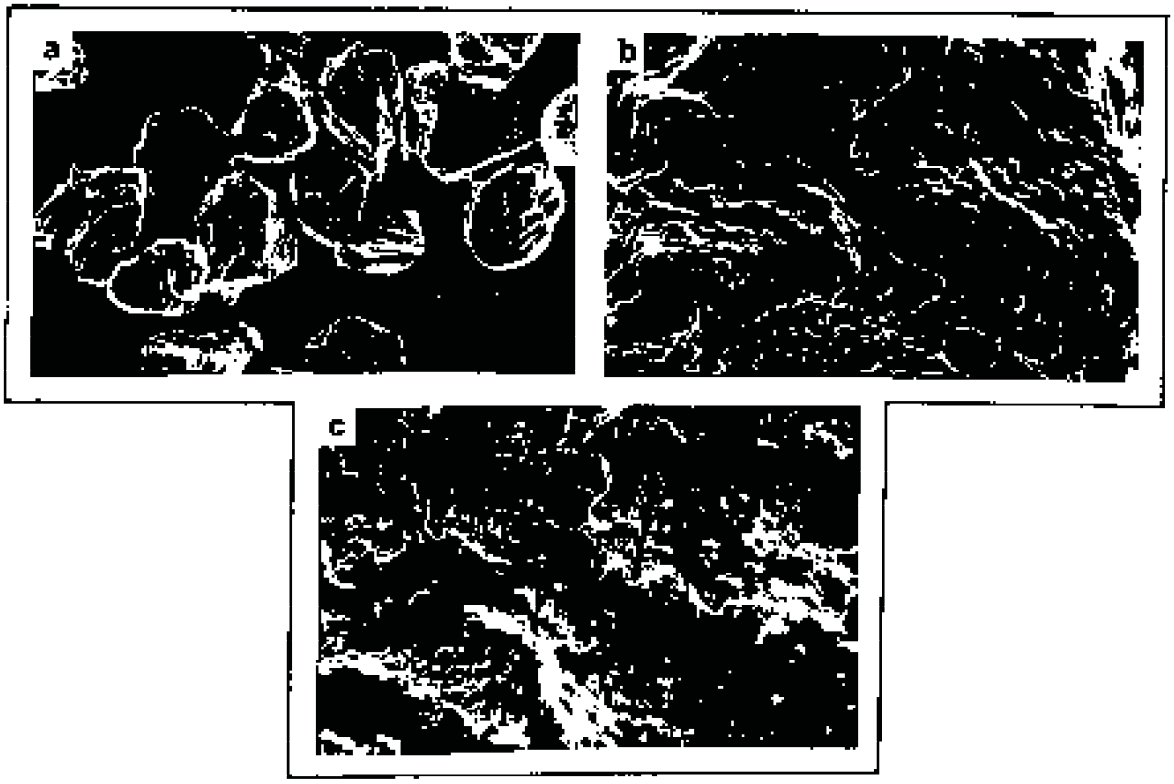


Figure 4.3 (ii) **Electron micrographs of the surface of a three hour leached Alloy C catalyst after WGSR**

a: MAG x 30
b: MAG x 200
c: MAG x 550

Considering Figures 4.2 (i) and (ii), it can be seen that evidence of alloy leaching is not visible at low magnification ((i) and (ii) a). Higher magnification and long leach times ((ii) b - d) reveal the formation of "nodules" on a *skeletal* or *striated* surface. The EDAX determined elemental composition of the "nodules" was found to be identical to the catalyst composition reported in Table 4.2. (Cu = 88.8wt%; Aℓ = 11.2wt%) and are therefore regarded as being part of the leach residue rather than of predominantly "unleachable" phases resistant to caustic action. It is well known (9, 10) that as a result of changing crystallite size profiles through the rim, extensive rearrangement of the copper occurs during leaching and it is therefore possible that the nodules (rich in copper) may be formed from concentrated deposits of caustic insoluble copper on the dendritic structures. This phenomenon is discussed in more detail in Section 4.3.1 (d). The surface of the 1 hour leached alloy consists of a uniform distribution of Aℓ and Zn (Figure 4.2

(i) d - e) indicating that non selective phase leaching probably occurs.

In Figures 4.4 (i) and (ii) electron micrographs together with zinc and aluminium mapping are presented to show the morphological development of "fresh" Raney catalysts prepared by varying the contact time to caustic solution.

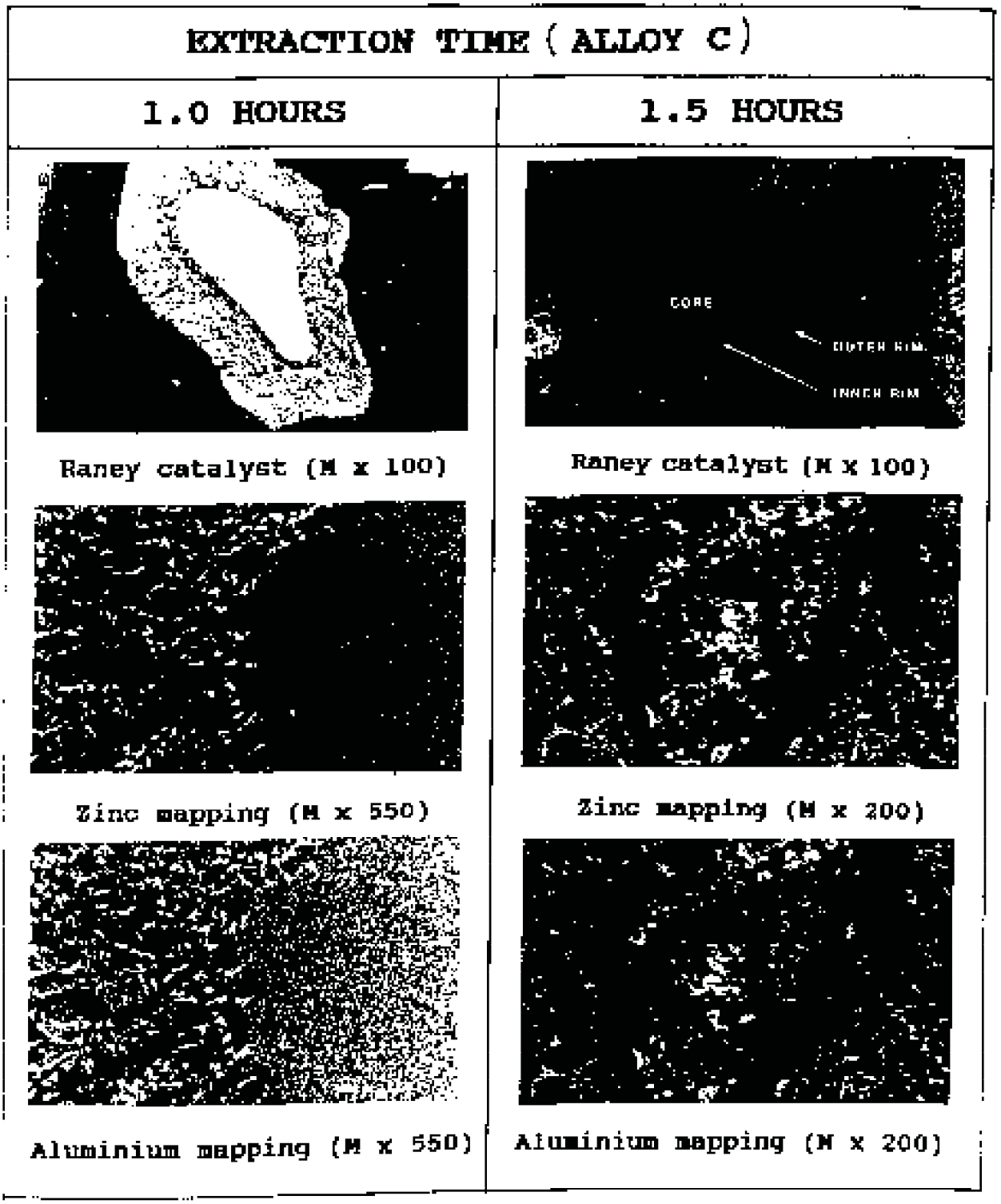


Figure 4.4 (i) Cross-sectional electron micrographs of Alloy C leached for 1.0 and 1.5 hours

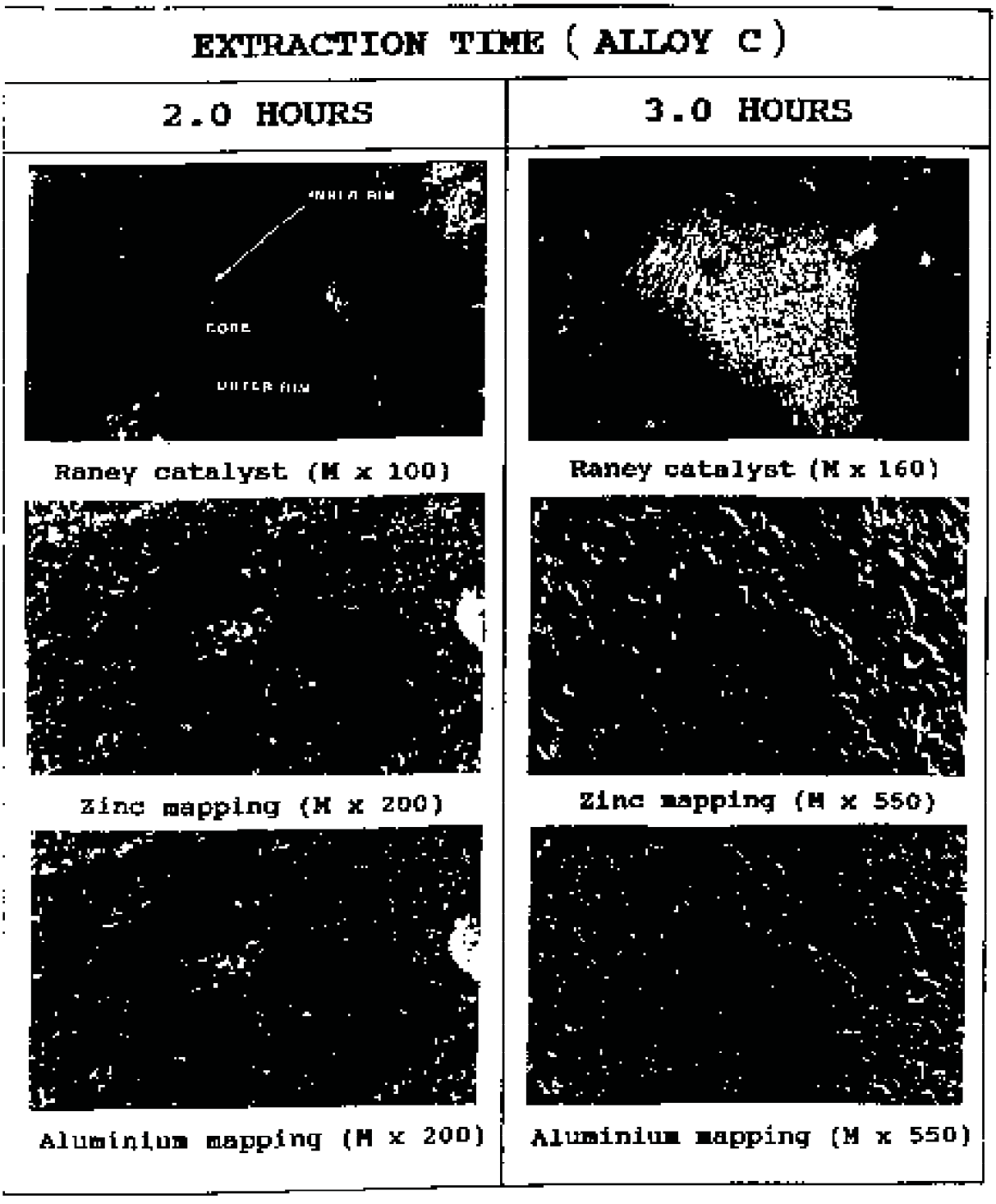


Figure 4.4 (ii) Cross-sectional electron micrographs of Alloy C leached for 2.0 and 3.0 hours

The electron micrographs in Figures 4.4 (i) and (ii) show that for reaction times up to 2 hours there is a clearly defined boundary between the reacted rim of porous Raney metal and a core of elemental composition similar to Alloy C (see Tables 4.1 and 4.2) indicating no leach reaction has as yet taken place in this region. The boundary is convoluted rather than planar. For all extraction times investigated, this boundary was found to be parallel to the original alloy surface. Partial leaching of alloys (for 1.5 and 2 hours) resulted in reaction product zones consisting of two layers, (clearly identifiable in Figures 4.4 (i) and (ii)), an outer layer of light coloured sponge material with interspersed black areas, and an inner band of intermediate shading of average diameter (30 - 40 μm) which is independent of alloy leach depth. Wainwright et al. (11) also observed that the reacted rim consisted of two distinct layers for leach times up to 2 hours. Microprobe analysis showed that the grains of the outer layer was essentially copper, whilst those in the inner layer were unreacted $Cu(Zn)Al_2$. The intergranular material had been leached completely to leave void space in both layers. This conclusion is consistent with the elemental mapping micrographs for 1.5 and 2.0 hour leached catalysts (Figures 4.4 (i) and (ii)) which show that the aluminium and zinc density is higher in the inner layer. After 3 hours no core was distinguishable from a rim, (Figure 4.4 (ii)) indicating that the particle had been leached to the centre. Andreev et al. (10) reported that the centre of a particles of diameter 1.2 - 2mm and chemical composition Cu(42.0) Zn(14.3) Al (43.5) were stable to leaching as a result of the ordered crystalline structure formed by slow quenching during alloy formation. The authors found that conditions of quick crystallization and contact with water were characterised by a defect structure which determined the higher reactivity of particles during leaching. For all catalysts in Figures 4.4 (i) and (ii), an even, well distributed concentration of Al and Zn in the outer layer of the reaction zone was observed.

The physical structure of the caustic reacted product residue before and after reactor testing is presented in Figures 4.5 (i) - (ii) and 4.6 (i) - (ii) respectively.

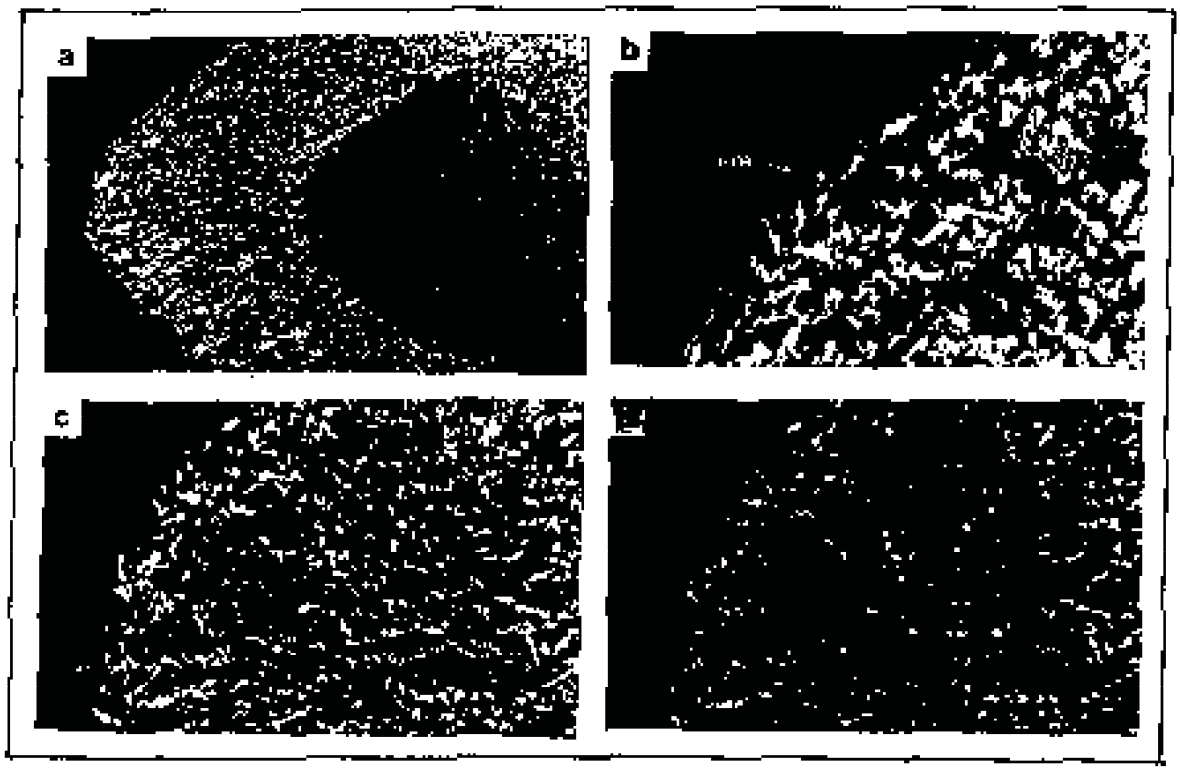


Figure 4.5 (i) Cross-sectional electron micrographs of the porous rim of a one hour leached Alloy C catalyst before WGSR

a: MAG X 220
b: MAG x 1000
c: Zn mapping (MAG x 550)
d: Al mapping (MAG x 550)